Effects of the terdiurnal tide on the Sporadic-E layers (Es) development at low latitudes over the Brazilian sector

Pedro A. Fontes[1,2*], Marcio T. A. H. Muella[1], Laysa C. A. Resende[3,4], Vânia F. Andrioli[3,4], Paulo R. Fagundes[1], Valdir G. Pillat[1], Paulo P. Batista[3], Alexander J. Carrasco[3,5]

[1]Universidade do Vale do Paraíba – Univap, São José dos Campos – SP, Brasil.

[2]Instituto Federal do Maranhão – IFMA, Bacabal – MA, Brasil.

[3]Instituto Nacional de Pesquisas Espaciais – INPE, São José dos Campos-SP, Brasil.

[4]State Key Laboratory of Space Weather, Beijing, China.

[5]Universidad de Los Andes, Mérida, Venezuela.

5   *Corresponding author*: Pedro A. Fontes (pedro.fontes@ifma.edu.br; pedro.fontes2@hotmail.com)

Abstract. Sporadic-E (*Es*) layers are patches of high ionization observed at around 100-140 km height in the E region. Their formation at low latitudes are primarily associated with the diurnal and semidiurnal components of the tidal winds via the ion convergence driven by the wind shear mechanism. However, recent studies have shown the influence of other tidal modes, such as the terdiurnal tide. Therefore, this work investigates the effect of terdiurnal tide-like oscillations on the

10   occurrence/formation of the *Es* layers observed over Palmas (10.17° S; 48.33° W; dip lat. -8.3°), a low latitude station in Brazil. The analysis was conducted from December/2008 to November/2009 by using data collected from a CADI (Canadian Advanced Digital Ionosonde) ionosonde. Additionally, the E Region Ionospheric Model (MIRE) was used to simulate the terdiurnal tidal component in the *Es* layer development. The results show modulations of 8-hour periods on the occurrence rates of the *Es* layers during all seasonal periods. In summer and autumn, we see three well-defined peaks in a superimposed

15   summation of the *Es* layer types per hour. We also observed that the modulation of the terdiurnal tide on the *Es* occurrence rates minimizes in December, the beginning of the summer season.

1 Introduction

Sporadic-E layers (*Es*) are thin and dense layers observed in the ionospheric E region at altitudes ranging from 100 to 140 km. The ion density of the *Es* layer is associated with molecular ions, mostly O_2^+ and NO^+, and the main metal ions, Fe^+, Mg^+,

20   and Na^+. Metal ions have a longer lifetime than the molecular ions, making the *Es* layers long-lasting (Whitehead, 1989; Plane, 2003).

The *Es* layers are divided into three different classes: equatorial layers, low- and mid-latitude layers, and the auroral or high-latitude layers. They are differentiated into types designated by the lowercase letters of the alphabet, such as Es_c (cusp), Es_f (flat), Es_h (high), Es_l (low), Es_q (equatorial), and Es_s (slant). The '*c*', '*h*', '*l*', and '*q*' types are formed in the

25   daytime, while the '*f*' type is usually nocturnal. Type '*h*' of *Es* occurs at higher altitudes, generally ranging between 120 and

140 km, and can appear and disappear suddenly, as well as evolving into type '*c*' at lower altitudes (Conceição-Santos et al., 2020). The '*l*' and '*f*' types generally occur at 100-110 km. Furthermore, the '*q*' type occurs near the magnetic equator around 100 km (Resende et al., 2017b; Conceição-Santos et al., 2020).

The *Es* layers occur at most latitudes and longitudes and have different mechanisms of formation that depend mainly on
30   magnetic latitude (Kirkwood and Nilsson, 2000). The vertical shear in the east-west component of horizontal winds (wind shear) is the most accepted theory to explain the formation of *Es* layers. According to this theory, a vertical convergence of the charged particles occurs by **U**×**B** forces, where **U** and **B** denote the horizontal wind and the Earth's geomagnetic field, respectively (Whitehead, 1961; 1989; Kirkwood and Nilsson, 2000; Haldoupis, 2012). The atmospheric tides are one of the possible sources of wind shears, which means that solar tides can strongly control the intensification of *Es* layers (Forbes and
35   Wu, 2006; Forbes et al., 2008; Moudden and Forbes, 2013). Solar tides are oscillations in the atmosphere that occur due to the absorption of infrared and EUV radiation by water (H_2O), ozone (O_3), and molecular oxygen (O_2) in the troposphere, stratosphere, and lower thermosphere. This absorption of radiation causes periodic heating and expansion of tidal amplitudes that grow exponentially in height as they are excited into regions of the lower thermosphere between the altitudes of 90 and 120 km (Forbes and Wu, 2006; Forbes et al., 2008; Smith, 2012; Pancheva et al., 2013).

40   The type of atmospheric tide can influence the development of the sporadic layers (Haldoupis and Pancheva, 2006; Haldoupis, 2012; Lilienthal et al., 2018). The convergence of the *Es* layer to altitudes whose vertical velocities of neutral winds correspond to zero may be driven by the global tidal wind system in the thermosphere (Haldoupis, 2012). The formation and variability of the *Es* layers may be related to the action of atmospheric waves in the lower thermosphere (McLandress, 2002a; 2002b; Haldoupis and Pancheva, 2006; Haldoupis, 2012). Haldoupis et al. (2004) used a time series of *Es* layer parameters scaled
45   from ionosonde data and found that the dominant amplitudes at the 3 to 36-hour period are the 24, 12, and 8-hour peaks associated, respectively, with the diurnal, semidiurnal, and terdiurnal atmospheric tides. Although the diurnal and semidiurnal tides play leading roles in the occurrence, altitude descent, and strength of *Es* layers, Haldoupis and Pancheva (2006) stressed that the terdiurnal tide can also have a contribution to the convergent shearing of the horizontal winds. In the mid-latitude station of Cyprus (35.0°N; 33.0°E), Oikonomou et al. (2014) observed the presence of terdiurnal tidal effects on *Es* layer that
50   prevailed only during summer months.

Additionally, Fytterer et al. (2014) used an atmospheric circulation model to support the observations of GPS radio occultation data, and the authors reported a well-pronounced peak in the *Es* layer occurrence at around 10° in both hemispheres associated with the migrating terdiurnal tide. In the Brazilian sector, Resende et al. (2016) and Resende et al. (2017a; 2017b) simulated the *Es* layer using a model called MIRE (E Region Ionospheric Model). They showed that the diurnal and semidiurnal
55   components are the main ones for forming the *Es* layer in this sector. However, they suggested that some discrepancies between the model and observational data might be due to the exclusion in the analysis of other tidal components such as terdiurnal and quarterdiurnal tides. It is worth mentioning that there are few studies in the literature concerning the role of the terdiurnal tidal modulation in the formation of *Es* layers, especially in equatorial and low-latitude regions (Haldoupis and Pancheva, 2006; Fytterer et al., 2014; Lilienthal et al., 2018).

60 Although our knowledge of tidal effects on *Es* layers has advanced over the last 20 years, there are still questions about the possible role of the terdiurnal tide on the formation of *Es* layers at low latitudes. Therefore, the present study analyzes the *Es* layer parameters obtained from data of an ionosonde installed in the low latitude station of Palmas, Brazil (10.17° S; 48.33° W; dip lat.-8.3), to investigate the modulation of the occurrence and formation of *Es* layers associated to the terdiurnal solar tide. In this context, the minimum virtual height (*h'Es*) and the top frequency (*ftEs*) parameters scaled from ionosonde data

65 were used in this analysis. Moreover, the types of the *Es* layers registered in the ionograms were classified according to the criteria established by the Union of Radio Science (Piggott and Rawer, 1972). During the analyzed period, it was possible to identify four distinct types of *Es* layers in the ionograms recorded by the ionosonde of Palmas. Finally, the E Region Ionospheric Model (MIRE) was used to simulate the effect of terdiurnal (8-h) tidal periodicities on the formation of the *Es* layers.

2 Methodology

2.1 Data Analysis

70 The ionosonde used in this work is the CADI (Canadian Advanced Digital Ionosonde) installed in Palmas, Brazil. This ionosonde type operates using a double delta antenna that serves both to transmit and receive the signal. After being processed, the received signal will register the *Es* traces in the ionograms. The transmitter used by the CADI system performs a frequency sweep in the HF range from 1 to 20 MHz with a power of 600 W and a pulse width of 40 s, which gives a height resolution of ±3 km (Gao and MacDougall, 1991; Huang and Macdougall, 2005). The ionograms were processed using the computer

75 software named UDIDA (Univap Digital Ionsonde Data Analysis), which has been employed to visualize the ionograms on a PC screen (Pillat et al., 2013).

The parameters of virtual height (*h'Es*), top frequency (*ftEs*), and type of the *Es* layers from the ionograms recorded every 5 min were scaled and classified. The classification of the different types of *Es* layers followed the criteria available in the U.R.S.I. Handbook of Ionogram Interpretation and Reduction (Piggott and Rawer, 1972). We used the months of December

80 of 2008 and January-February of 2009 as representative of summer; the months of March, April, and May of 2009 as representative of autumn; the months of June, July, and August of 2009 as representative of winter; and finally, the months of September, October, and November of 2009 as representative of spring.

2.2 The MIRE Model

The extended version of the E Region Ionospheric Model (MIRE) was used in this study to calculate the *Es* layers' electronic

85 density profile (Resende et al., 2017a; Conceição-Santos et al., 2019). The MIRE uses the continuity equation to calculate the sum of the ionic density for the main constituents, such as $NO^+, O_2^+, O^+, N_2^+, Fe^+$, and Mg^+. The model calculates the time derivative of the ion density, $\partial(N_i)/\partial t$, which depends on the production, p_i, the loss, l_i, and the transport term, $\partial(V_{iz}[N_i])/\partial z$. Therefore, the electronic density profile is given by the sum of the molecular and metal ions, as shown in

Equation 1. The simulations are obtained in a space-time of approximately 0.2 km height every 2 minutes between 00-24 UT

90 for altitudes between 86 and 140 km, assuming photochemical equilibrium of the species as initial conditions for the numerical equations to be solved until ion convergence is reached (Carrasco et al., 2007; Resende et al., 2016; 2017a; 2017b; Conceição-Santos et al., 2019; 2020).

$$n_e = [O_2^+] + [NO^+] + [O^+] + [N_2^+] + [Fe^+] + [Mg^+]. \tag{1}$$

For the transport term in the continuity equation, the MIRE uses the equation of motion that depends on the meridional (U_x) and zonal (U_y) wind components, and the electric field $(E_{x,y,z})$, as given in Equation 2.

$$\boldsymbol{V}_{iz} = \frac{\omega_i^2}{(v_{in}^2 + \omega_i^2)}\left[cosI.sinI.U_x + \frac{v_{in}}{\omega_i}.cosI.U_y + \frac{1}{v_{in}}\frac{e}{m_i}.cosI.sinI.E_x + \frac{e}{\omega_i m_i}.cosI.E_y \right.$$
$$\left. + \frac{e}{v_{in} m_i}.\left(\frac{v_{in}^2}{\omega_i^2} + sin^2 I\right).E_z\right], \tag{2}$$

95 where ω_i is the ion's gyrofrequency; v_{in} is the ion-neutral collision frequency; I is the magnetic inclination angle; m_i is the ion's mass; and e is the ion's electric charge. The coordinate system is composed of the x-axis pointing south, the y-axis pointing east, and the z-axis pointing up.

In this work, the wind data used in MIRE was obtained by the SkiYMET meteor radar installed in the OLAP observatory at São João do Cariri (7.23° S; 36.32° W; dip lat. -22.22). The SkiYMET radar monitors the meteor echoes for altitudes ranging

100 from 80 to 100 km (Hocking, 2004; Buriti et al., 2008; Andrioli et al., 2009). However, the height range of interest in this study at MIRE is between 86 and 140 km (Resende et al., 2017a; 2017b). Thus, between 100 and 120 km, the model performs a wind parameter adjustment based on wind shear theory to analyze the dynamics of the *Es* layer, and the wind equations were expanded up to 120 km according to a Lorentz curve fit for diurnal, semidiurnal, and terdiurnal tides. The vertical wavelengths $\lambda_{x,y}$ are considered constant up to ~100 km. Above that altitude, the tidal winds tend to have a non-constant wavelength

105 (Lieberman, et al., 2013; Conceição-Santos et al., 2020). In fact, the wavelength fit in MIRE tends to infinity above 120 km. Finally, the wind profiles agreed with the previous study performed with Wind Image Interferometer (WINDII) aboard the Upper Atmosphere Research Satellite (UARS) between 90 and 270 km seen in Lieberman et al. (2013). Equations 3 and 4 represent, respectively, the meridional and zonal wind components, given by:

$$U_x(z) = U_{x0}(z).cos\left(\frac{2\pi}{\lambda_x}(z - z_0) + \frac{2\pi}{T}\left(t - t_{x0}(z)\right)\right), \tag{3}$$

$$U_y(z) = -U_{y0}(z).sin\left(\frac{2\pi}{\lambda_y}(z - z_0) + \frac{2\pi}{T}\left(t - t_{y0}(z)\right)\right), \tag{4}$$

where $U_{x0}(z)$ and $U_{y0}(z)$ are the wind amplitudes at height z; λ_x and λ_y are the wavelengths for the respective meridional and zonal components of the diurnal, semidiurnal and terdiurnal tides; z_0 is a reference height (100 km); $t_{x0}(z)$ and $t_{y0}(z)$ are the wave phases; T is the tidal period, which can be diurnal (24h), semidiurnal (12h), or terdiurnal (8h).

It is important to mention that this work is the first study in which the terdiurnal tide was implemented in the MIRE model by using the SkiYMET wind profiles obtained from data collected at São João do Cariri. These data were used as representative of the winds over the observatory of Palmas since no other measurements at any closer station were available simultaneously with the ionosonde observations. Thus, the inferred neutral winds and atmospheric tides were included in Eqs. (2-4) of MIRE to simulate the Es layer dynamics over Palmas.

3 Results and Discussion

3.1 Terdiurnal Tide Periodicities in Es Layer Occurrences

Figure 1 shows the temporal variation (in UT) of the percentage occurrence of the *'h'*, *'c'*, and *'f/l'* types of Es layers during the summer solstice months of 2008/2009. The occurrences of the *'f'* and *'l'* types were grouped into one since both have nearly the same ionogram profile; however, the *'l'* type manifests only during the daytime, and the *'f'* type is typically nocturnal (Conceição-Santos et al., 2020). From December 2008 to February 2009 (summer), a total of 48 days of data was recorded by the ionosonde of Palmas, which corresponds to 2,859 ionograms. The daytime occurrence of Es layers was 65.58% (156.25 hours), while 34.42% (82 hours) occurred during nighttime. The $Es_{f/l}$ types were the most frequent, with an overall rate of 72.61% (173 hours).

Notice that the first peak of the Es layer occurrence is observed between about 01-02 UT (LT = UT – 3.0h), and the $Es_{f/l}$ layers are predominant during nighttime. Then a sharp decrease occurs near dawn at 08 UT reaching occurrence rates of less than ~7%. Approximately 8 hours after the first peak, the Es layers percentage of occurrence increases markedly, reaching ~50% between about 10-11 UT. This second peak coincides with the increase in the occurrence rates of the *'c'* and *'h'* types of Es layers. The Es_c and Es_h layers are formed starting at dawn, after 09 UT, and cease at dusk around 20 UT. The Es_c type corresponds to 13.47% (total of 32.08 hours), while the Es_h type corresponds to a rate of 13.92% (total of 33.17 hours). It is clearly noticed that the Es_h layer predominates over the other Es types between around 10-12 UT. After this second peak in the occurrence rate, Es types of the percentage of occurrence starts to decrease again and reaches values of ~7% between about 15-16 UT. However, after 17 UT, the occurrence rate starts to increase again and attains the third peak between around 19-21 UT with values of ~41%. The three peaks observed in the plot of occurrence rates of Es layer types with 8-h periodicities suggest a modulation associated with the terdiurnal tide during the summer period.
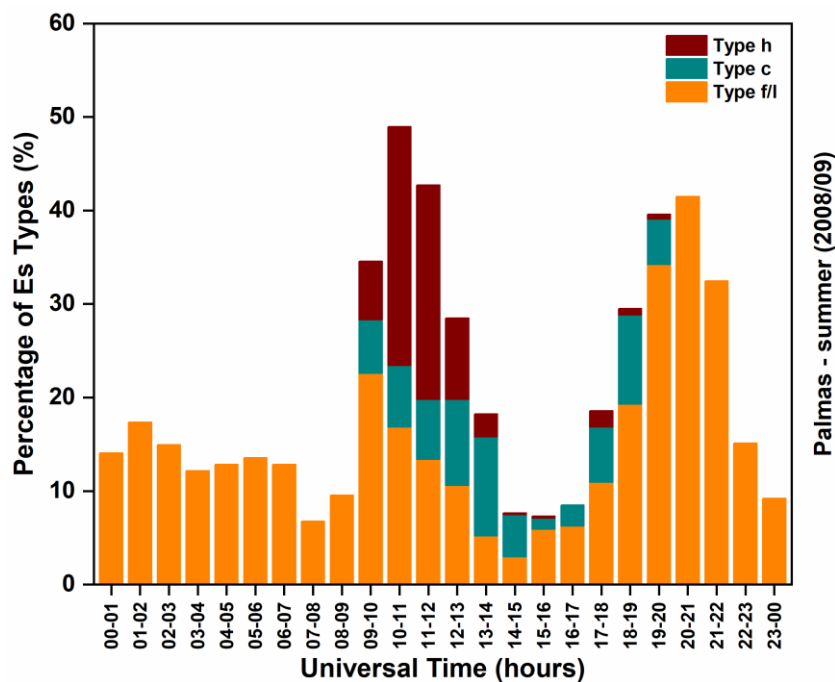
Figure 1: Temporal variation of the *Es* layer occurrence rates divided in different types over Palmas during the summer solstice months (from December/2008 to February/2009).

The analysis of the temporal occurrence of *Es* layer types over Palmas was extended for the autumn, winter, and spring seasons, as seen in Figure 2. In this figure, we show the occurrence rates for autumn (top panel), winter (middle panel), and spring

140 (bottom panel). As noted earlier for the summer, the $Es_{f/l}$ types were also predominant during nighttime, and the Es_c and Es_h types occurred only during daytime. Except for the interval between 11-12 UT in winter when the $Es_{f/l}$ layers were predominant. Also, in autumn, we observed three well-defined maxima in the occurrence rate of *Es* layer types, whereas in the winter and spring months, the first peak is not well defined. However, we observed clear second and third ones at around 10-12 UT and 18-20 UT, respectively, indicating the possible influence of the terdiurnal tide. The slight increase in the occurrence

145 rate between around 03-04 UT during the spring season might suggest that besides the dominant terdiurnal tidal periodicities, there was also a weaker quarterdiurnal (6-h) oscillation affecting the *Es* layer development. By comparing the results shown in Figures 1 and 2, it is clearly noticed that the another peak of ~47% was observed between around 10-11 UT during the spring season. Furthermore, the larger amplitudes of the *Es* layer occurrence rates associated with the terdiurnal tide modulation were observed during the summer and spring months.
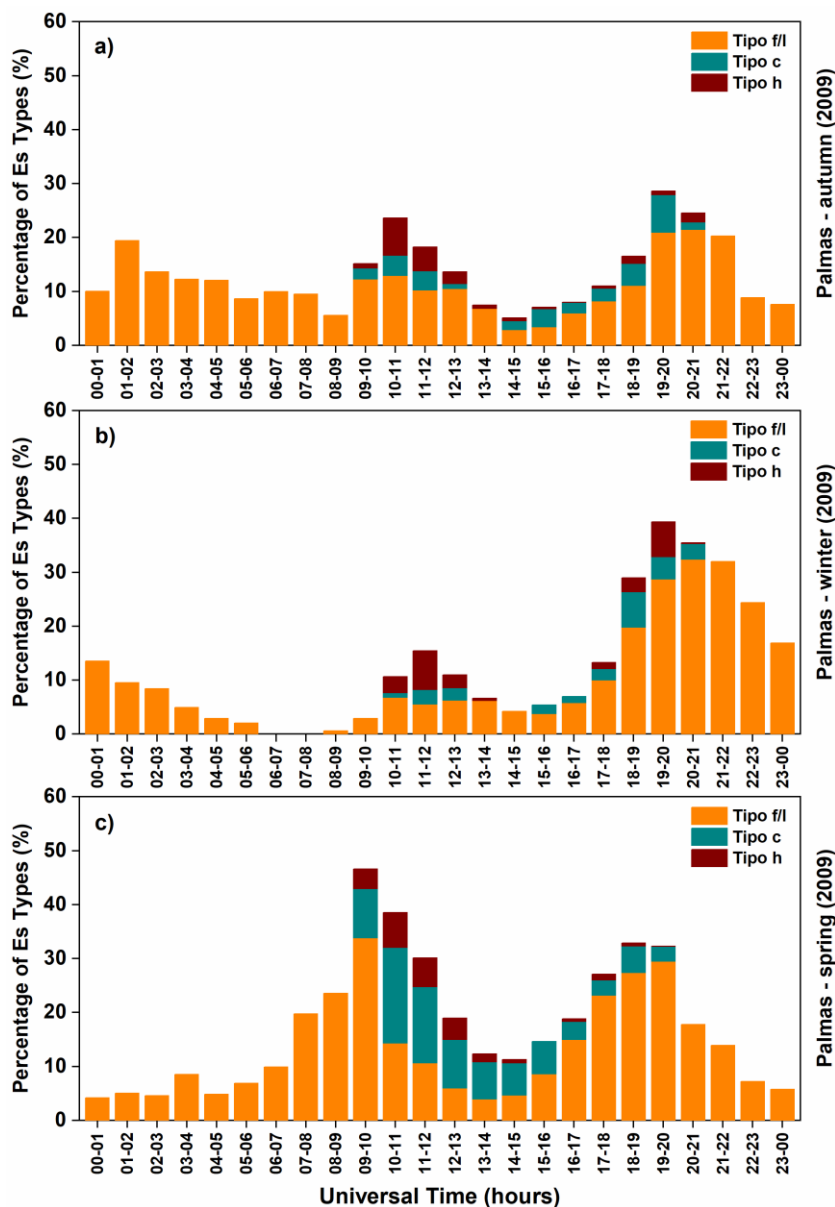
Figure 2:Temporal variation of the *Es* layer type occurrences over Palmas during autumn (panel a), winter (panel b), and spring (panel c) months of the year 2009.

150   Figure 3 depicts the temporal variation of the *Es* layer (*h'Es*) for the '*h*', '*c*', and '*f/l*' types during the four seasonal periods at Palmas. It is seen from Figure 3 that the Es_h layers were formed at higher altitudes between around 130 and 150 km, whereas the Es_c layers were observed at altitudes ranging from 110 to 130 km. As expected, the Es_c and $Es_{f/l}$ layers were mostly observed at altitudes below 110 km, although during some specific hours at all seasons, they attained heights of ~130 km. The Es_h layer tends to move down to lower heights in the E region, changing into types '*c*' or '*l*' when they reach 100 km

155 (Conceição-Santos et al., 2020). Another relevant aspect to be observed in Figure 3 is related to the distribution of *h'Es* during

the times of maximum occurrence rate of the *Es* layer types, which is possibly associated with the terdiurnal tide. During the

peaks in the frequency of occurrence of *Es* layers at around 10-12 UT and 18-20 UT, Figure 3 reveals for all seasons that the

Es layers attained their highest altitudes. Otherwise, during the time of the first peak at around 01-02-UT, it was not evidenced

significant changes in the heights of the $Es_{f/l}$ layers. However, it seems that the terdiurnal tidal oscillations had some role in

160 the formation of the Es_h layers during the daytime.
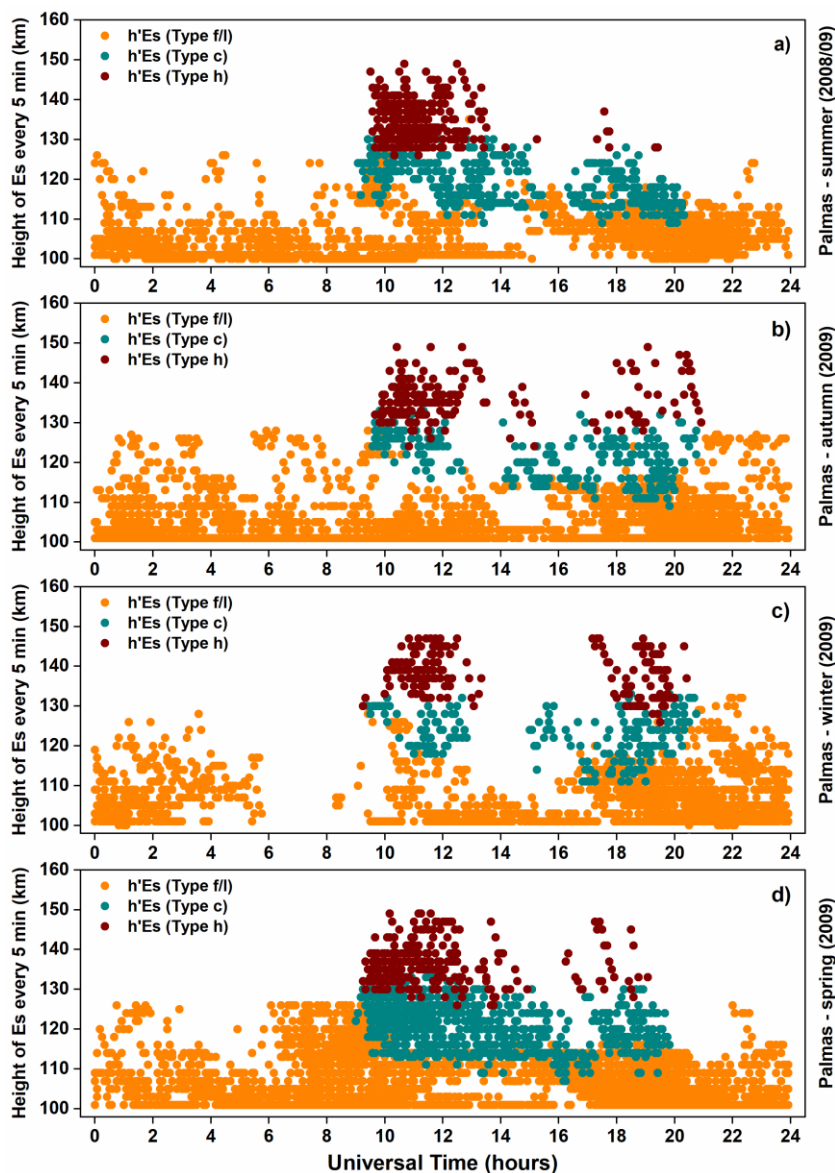
Figure 3: Virtual height distribution of the *Es* layer types as function of time (in UT) over Palmas during summer (panel a), autumn (panel b), winter (panel c), and spring (panel d).

As it is already known, tides are the major sources of vertical wind shear (Jacobi and Arras, 2019). Thus, tidal-like structures

165 are expected to influence the occurrence rates of *Es* layers strongly. As noticed in Figure 3, most of the *Es* layers are

concentrated at heights below 120 km. According to Fytterer et al. (2014), the influence of the terdiurnal oscillations on *Es*

formation and evolution is restricted to heights between around 100-120 km. Thus, in this height range, the terdiurnal tidal

oscillations may have a similar amplitude to the diurnal and semidiurnal tides (Zhao et al., 2005; Venkateswara Rao et al.,

2011; Moudden and Forbes, 2013; Fytterer et al., 2014), and can also play an important role in modulating the *Es* layers.
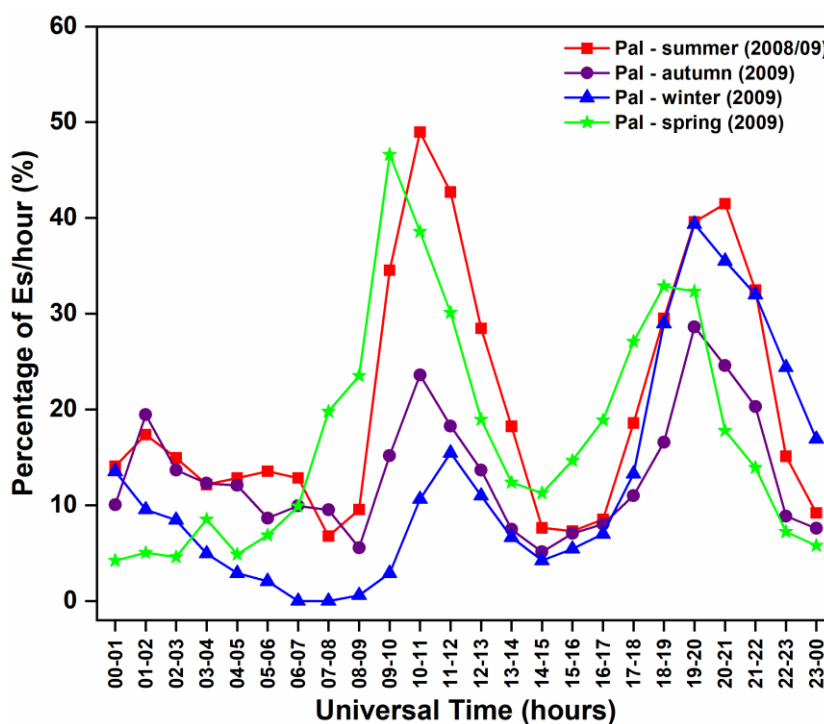
Figure 4: Comparison of the total percentages of occurrence of the *Es* layers over Palmas during the summer, autumn, winter, and spring seasons.

170 All types of *Es* layers were grouped to calculate the temporal variation of the total percentage of occurrence of the *Es* layers

observed in Palmas during the four seasons. These results of the total occurrence obtained during summer (red line), autumn

(purple line), winter (blue line), and spring (green line) are shown in Figure 4. The three maximum values in the total

occurrence rate of the *Es* layers during the summer and autumn months agree with the results observed before in Figs. 1 and

2. As already seen, these peaks are approximately 8 hours apart from each other, revealing a possible modulation by the

175 terdiurnal tide. Analogously to what was observed in Figure 2, during winter, only two maxima in the total percentage of

occurrence are noticed, being one at around 11-12 UT, and another at about 19-20 UT. As for the spring, a maximum in the

occurrence rate was observed during the morning between approximately 09-10 UT, and ~8 hours later, another maximum

was observed at dusk between around 18-20 UT. However, a small peak of ~8.5% was observed in the total percentage rate

between around 03-04 UT during the spring, which reveals again the possible effect of a weaker 6-hour tidal mode embedded

180   in the temporal occurrence rate of the *Es* layers.
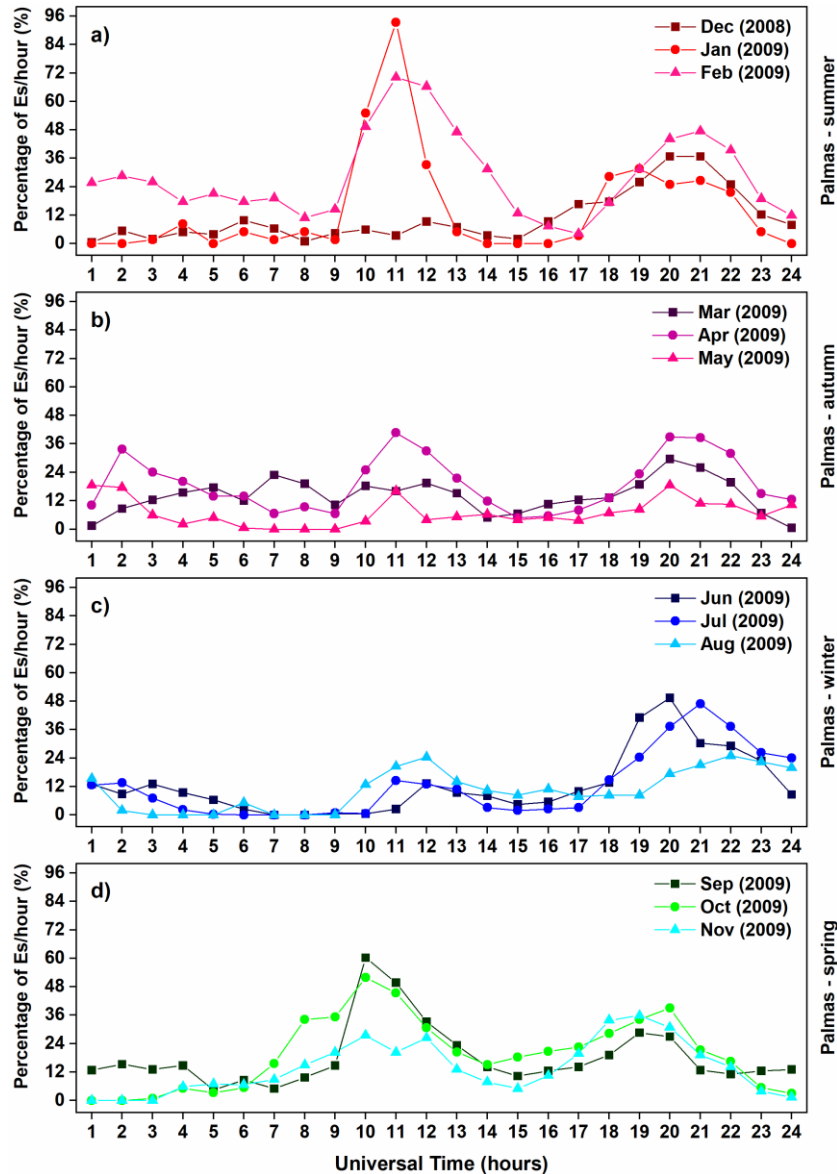
Figure 5: Temporal variation of the *Es* layer occurrence over Palmas showed into individual month during the summer (panel a), autumn (panel b), winter (panel c), and spring (panel d).

Figure 5 shows the monthly percentage of occurrences of *Es* layers divided by seasons. In summer (Figure 5(a)), the terdiurnal modulation is dominant during February/2009. On the other hand, in December/2008 and January/2009, the first peak in the occurrence rate observed previously at around 01-02 UT is practically absent. This is probably related to the tendency for the amplitude of the migrating terdiurnal tide to increase, generally from January to March within ±10° of latitude (Moudden and

185 Forbes, 2013; Pancheva et al., 2013). Thus, the maximum peaks in the occurrence rates observed in February of 2009 are higher than those observed in December/January, owing to the fact that this month is when the summer solstice starts in the Southern Hemisphere. This result also agrees with Guharay et al. (2013). They showed a smaller terdiurnal tidal range for the months of December/January and an increase of this compontent in February at low latitude in the Brazilian sector.

During autumn (Figure 5(b)) the 8-h tidal oscillations are noticed in the results of April and May. Notice that the three peaks
190 in the occurrence rates in April are higher than in the other months. Unlike the results shown in Figures 2 and 4, Figure 5(c) reveals a weaker peak in the percentage of occurrence (~12%) between around 01-03 UT, a clear second peak after 8-h, and a strong peak at approximately 19-21 UT. The total percentage of occurrence (Figure 4) between 01-05 UT during winter was strongly influenced by the occurrence rate observed in August. Guharay et al. (2013) also found a significant increase in tidal amplitude in the autumn and minimum values for winter and early summer. Finally, in spring, the modulations associated with
195 the terdiurnal tide are marked during September, October, and November.

The temporal variation of the total percentage of occurrence of *Es* layers was plotted in intervals of 20 min, as shown in Figure 6. The results for summer (red), autumn (purple), winter (blue), and spring (green) are shown as line plots. Then a nonlinear polynomial regression was applied to fit the occurrence rate curves for each season (black lines). The shadowed bands in the fitted curves denote the 95% confidence interval of the best-fitted parameters. It is possible to note that the curves of percentage
200 rates are mostly within the 95% confidence range of the nonlinear curves. However, when the peaks in the occurrence rates are above the 95% level of confidence reveals the most significant effect of the terdiurnal tide on the formation and dynamics of *Es* layers. It is worth noting from Figure 6 the 8-h periodicities in the fitted curves of all the seasonal periods. During winter, the first peak at around 02-03 UT is not as pronounced as in the other seasons, but now it is more perceivable than Figures 2 and 4 and also depicts the pattern seen in Figure 5 for June and July. According to Du and Ward (2010), the maximum
205 amplitudes of the terdiurnal tide are confined between ±50° of latitude and tend to occur in winter between 80 and 100 km of altitude. So as the *Es* layers over Palmas were observed above 100 km, this may partly explain why the terdiurnal oscillations were less pronounced in winter.

The results in Figure 6 also agree with the study of Moudden and Forbes (2013), who analyzed 10 years of data and highlighted that migrating terdiurnal tide reaches higher amplitudes near the equator at altitudes above 100 km, but with higher amplitudes
210 for the Southern Hemisphere. Pancheva et al. (2013) also analyzed 8 years (2002-2009) of terdiurnal tidal oscillations and found that between latitudes of ±10°, the amplitude of the terdiurnal tide at an altitude of ~90 km had a maximum in the month of February and that at 110 km altitude at low latitudes (±30°) had a maximum amplitude during the summer and winter.
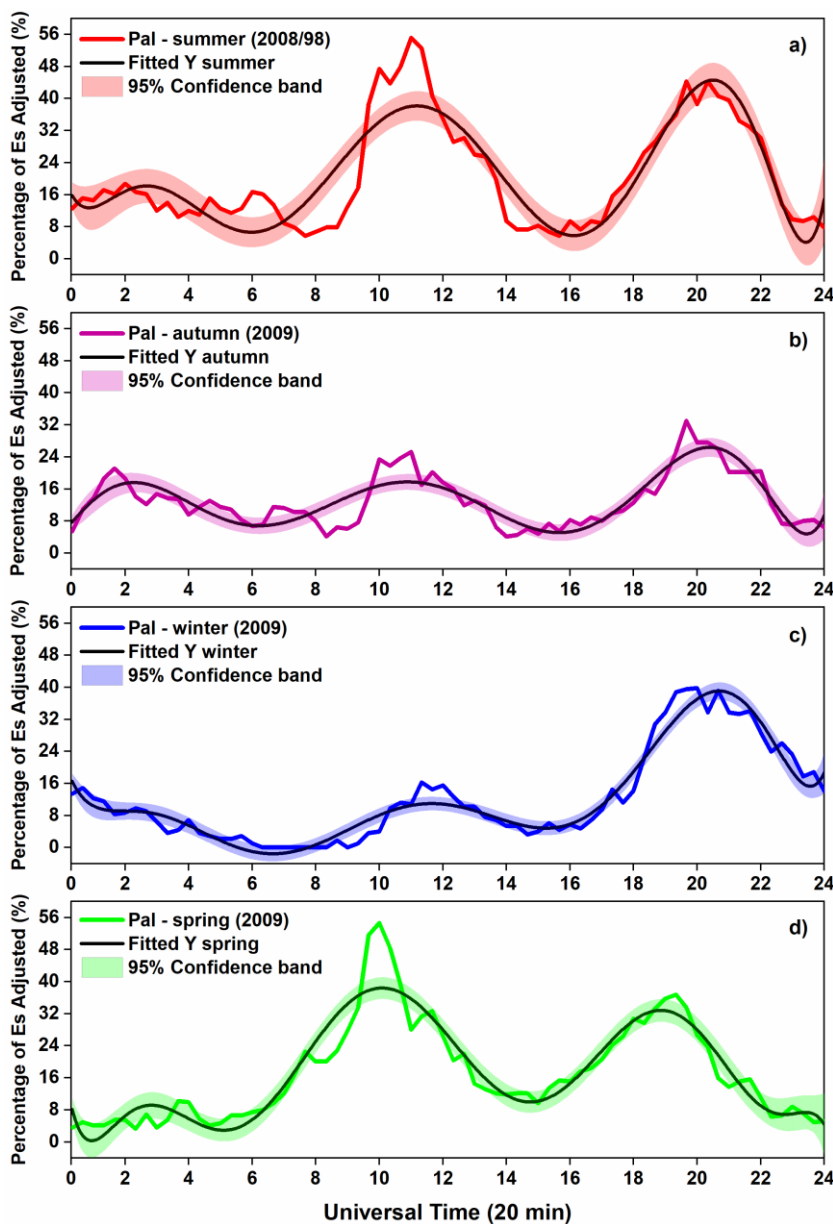
Figure 6: Temporal variation of *Es* layers occurrences obtained in intervals of 20 min during summer (red line/panel a), autumn (purple line/panel b), winter (blue line/panel c) and spring (green lone/panel d) seasons. The black lines in the panels are the fitted curves of the occurrence rates by applying a nonlinear regression. The shadowed bands in the fitted curves denote the 95% confidence interval of the best-fitted parameters.

The 3D colormap surfaces in Figure 7 present the top frequencies of layer *Es* (*ftEs*) distributed per day (in UT) for the summer, autumn, winter, and spring seasons. The color assigned in the graphs is related to the *Es* layer intensity. It is important to mention here that there are some gaps in the data during the summer and the winter, corresponding to zero on the scale of values of the *ftEs* but not affecting the previous results presented here.
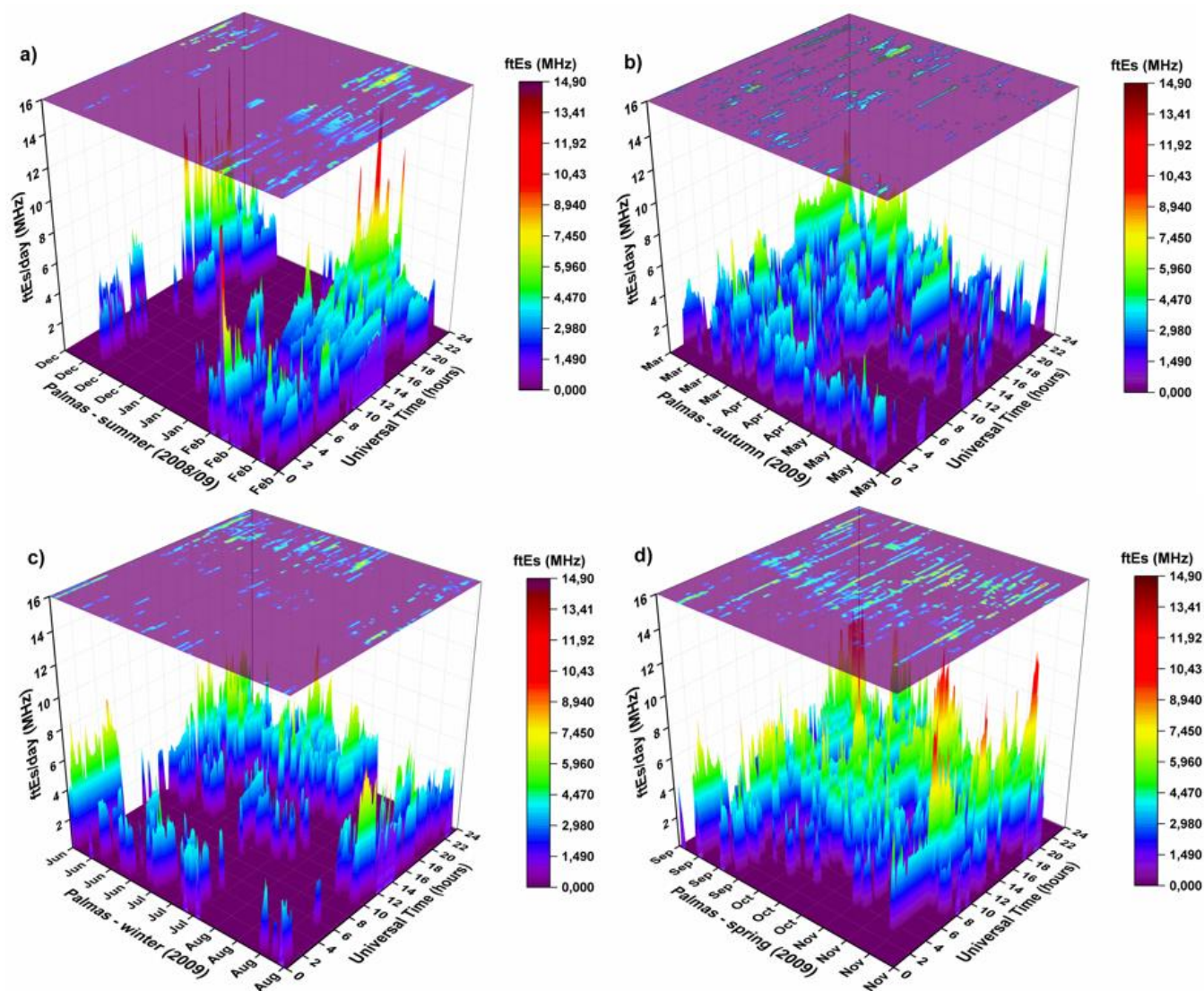
Figure 7: Top frequencies of the *Es* layers (*ftEs*) for the summer (panel a), autumn (panel b), winter (panel c), and spring (panel d) of the *Es* layer occurrence totals over Palmas.

Figure 7 reveals that in autumn and winter, the *ftEs* magnitudes were lower than those observed during the summer or spring months. Such *ftEs* values are almost always below 10 MHz. On the other hand, it was observed that *ftEs* values were above 10 MHz during spring. Summer presented the highest *ftEs* values in the late afternoon, whose maximum intensity was 14.9 MHz (20 UT). This maximum intensity of the *ftEs* was detected in early February (02/06/2009) and some days in December 2008. We believe that the high values of the *ftEs* observed here in early February may be due to the event of sudden stratospheric warming (SSW) that occurred between late January and early February of 2009 (Wang et al., 2011; Fuller-Rowell et al., 2011). This SSW event had global effects on the semidiurnal (SW2), terdiurnal (TW3) tidal amplitudes, and planetary waves (PW1 and PW2) (Wang et al., 2011; Fuller-Rowell et al., 2011; Lin et al., 2012; Jin et al., 2012). It is well known that during a SSW

the planetary waves can propagate vertically into the lower thermosphere and interact with the tides that dominate the dynamics in the ionospheric region. Thus, they can influence the development of the *Es* layers formed at this altitude (Liu and Roble, 2002; Lin et al., 2012; Fytterer et al., 2014). Wang et al. (2011) showed a SW2 tidal growth peaking after the SSW maximum and a TW3 decrease in the Southern Hemisphere. Subsequently, between 100-120 km altitude at 20-60º S, the rapid growth of

230 tidal amplitude TW3 and a considerable decrease of SW2 occurred. The authors attributed to a transfer of energy from the SW2 to the TW3 tide in both hemispheres. Jin et al. (2012) showed that a notable increase in TW3 amplitude occurred at 115 km altitude after the SSW at low latitudes between 0-30° S. Therefore, the prominent peak in the *ftEs* (Figure 7(a)) may indicate further evidence of the influence of the terdiurnal tide on the development of the *Es* layer.

The results of the *Es* layer intensity do not provide a conclusion that terdiurnal tide is influencing the densities, as is shown in

235 height. However, we found some correlation between the strong *Es* layer and the most terdiurnal modulation, as seen during the summer. Thus, we used a model to analyze the terdiurnal tide role in the *Es* layer behavior that will be present in the following section.

3.2 E Region Simulations

The simulations of the ionospheric electron density profiles (in logarithmic scale) between 86 and 140 km concerning the Universal Times are shown in Figure 8. We considered in the simulations the three tidal structures (semidiurnal, diurnal, and

240 terdiurnal periodicities) for the zonal and meridional wind components. The panels on the left column of Figure 8 refer to the results of diurnal and semidiurnal tides (D+S), while the panels on the right column show the simulation results considering the diurnal, semidiurnal, and terdiurnal tides (D+S+T). We selected data from different months to represent each seasonal period: December 2008 (summer/topmost panels a), April 2009 (autumn/panels b), July 2009 (winter/panels c), and October 2009 (spring/panels d). These months were chosen because, during the period analyzed here, they presented better diurnal,

245 semidiurnal, and terdiurnal wind data estimations from meteor radar observations at São João do Cariri, and there is already a study on the terdiurnal tide with data from this station in the Brazilian sector that can be found in Guharay et al. (2013). As we mentioned before, these wind data were used as input to the MIRE model. The thin traces of enhanced electron density seen in the plots of density profiles in Figure 8 denote the presence of the *Es* layers.
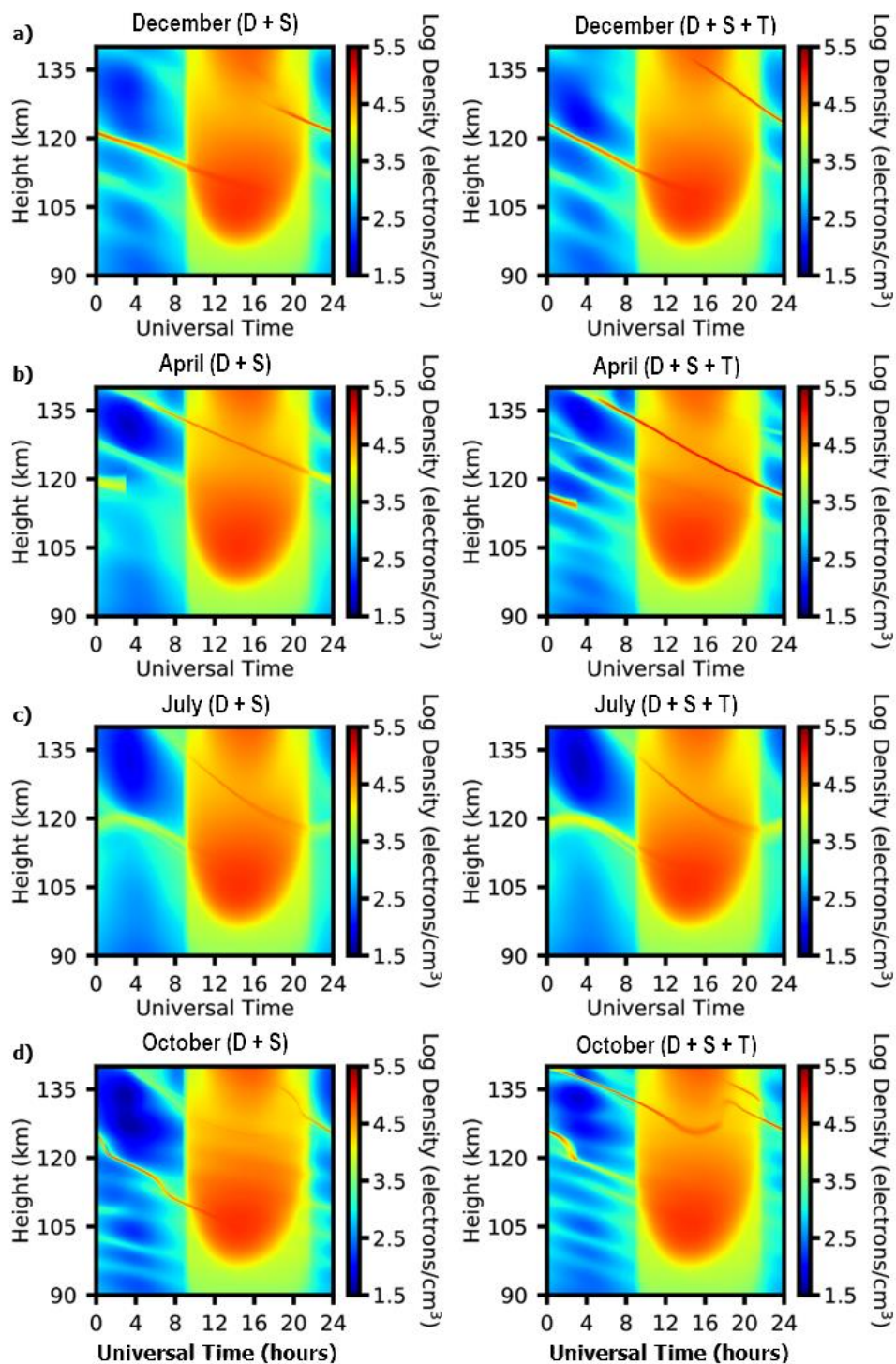
Figure 8: Density profiles of the *Es* layers simulated by MIRE during (a) December (summer), (b) April (autumn), (c) July (winter), and (d) October (spring).

In the plots of electron density profile shown in Figure 8(a) for December (summer), it is possible to see that when only diurnal
and semidiurnal tides (D+S) are considered in the simulations, the *Es* layer is formed at 16 UT just below 130 km altitude.
This *Es* layer tends to move downward throughout the night and reaches an altitude of ~115 km near dawn at 09 UT. During
the day, it continues to descend slowly until reaching ~110 km at around 16 UT. The density of this *Es* layer has a maximum
value of ~$10^{4.5}$ electrons/cm^3. When adding the terdiurnal tide (D+S+T) in the simulations, the results in the right panel of
Figure 8(a) clearly reveal that the layer is formed at higher altitudes above 135 km at around 14 UT. Analogously to what was
observed from the (D+S) simulation, the *Es* layer descended continuously and reached ~110 km 24-hours later. It is also noted
an intensification of the maximum *Es* layer density to ~$10^{5.0}$ electrons/cm^3.

The results of the MIRE simulations for April (autumn) are presented in Figure 8(b). The D+S simulation shows a thick *Es*
layer starting at around heights of more than 138 km and descending continuously, reaching ~120 km altitude at 24 UT. The
maximum density of this *Es* layer is about ~$10^{5.0}$ electrons/cm^3. By adding the terdiurnal tide (D+S+T) into the simulation,
the results show that the most intense *Es* layer forms at about ~140 km altitude at 03 UT and moves downward. Notice that
along almost its entire descent trajectory, the layer density is notably larger (~$10^{5.5}$ electrons/cm^3) compared to the D+S
simulation.

The panels in Figure 8(c) for July (winter) show similar results from the D+S and the D+S+T simulations regarding the height
of formation and descent of the *Es* layers. In both simulations, the *Es* layer is formed at around 06 UT at heights of ~140 km.
As the layer descends throughout the day, the electron density increases ~$10^{4.5}$ electrons/cm^3 for the D+S simulation and ~$10^{5.0}$
electrons/cm^3 for the case D+S+T simulation. From 22 UT until around 04 UT, the layer stops descending, becomes thicker,
and its electron density decreases to ~$10^{4.0}$ electrons/cm^3. Furthermore, it presents a slight rise from ~117 to 122 km. Then the
Es layer starts to descend again until pre-sunrise hours.

Finally, the MIRE simulations for the month of October (spring) present in the panels of Figure 8(d) a very distinct diurnal
behavior between the D+S and D+S+T simulations. The *Es* layer in simulation due to D+S is formed during daytime at ~140
km. This layer moves to downward, reaching ~125 km at 24 UT. The results show that this layer continues to move downwards
throughout the night and remains until around 12 UT when it attains ~107 km. A marked feature observed along the descent
course of this layer is the presence of oscillations in its height. The maximum electron density was ~$10^{4.5}$ electrons/cm^3. Such
oscillations seen in the traces of *Es* layers for both plots of panels 8(d) have already been reported by Conceição-Santos et al.
(2020) as possible interactions between gravity/planetary waves and tides.

Additionally, according to Lilienthal et al. (2018), the terdiurnal tide can only occur if both the diurnal and the semidiurnal
tides show considerable amplitudes. This is consistent with our results since the terdiurnal tide alone was not able to generate
Es layers in the simulations (not shown here). Moudden and Forbes (2013) compared diurnal, semidiurnal, and terdiurnal tides,
and they stated that there is a strong possibility that the non-linear interaction between diurnal and semidiurnal tides is the
main source of terdiurnal tide formation. Thus, depending on altitude and latitude, the terdiurnal tide can exhibit amplitudes
with significant magnitude, and this can play an important role in the dynamics and modulations of *Es* layer densities (Moudden
and Forbes, 2013; Pancheva et al., 2013; Fytterer et al., 2013; 2014).

By using radio occultation (RO) data, Fytterer et al. (2014) performed a global analysis of the effect of the terdiurnal tide on the occurrences of the *Es* layers. They used data collected in the period from 2006 to 2012 during the four seasonal periods for latitudes of $\pm 60°$ and altitudes ranging between 85 and 115 km. The authors found two amplitude maxima in the terdiurnal tide signature over the *Es* layers during the solstice that maximize between 10° and 40° latitudes in both hemispheres. In addition, they also found similar behavior for low-latitude equinox conditions in both hemispheres for altitudes above 100 km. Thus, the intensification of the *Es* layer densities obtained here from MIRE simulations are in accordance with the observations in Fytterer et al. (2014). In summer and spring, the simulations showed a more intense *Es* layer variation when added the 8-h tide. This behavior can cause high *ftEs* to be observed in such seasons. Finally, our results show that the inclusion of the terdiurnal tide caused an increase in the electron density of the *Es* layers for all seasonal periods.

4 Conclusion

This paper presented an analysis of the effect of terdiurnal tidal modulation on the occurrence rate of the *Es* layers observed during the years 2008/09 in Palmas, a low latitude station located in Brazil. We used ionosonde data and simulations to investigate the effect of terdiurnal (8-h) tidal periodicities on the formation of the *Es* layers during different seasonal periods. The main results of this study are summarized as the follows:

1. The $Es_{f/l}$ is the most common type found in all seasons, and types Es_c e Es_h appear exclusively in the daytime over Palmas, agreeing with the previous results shown in Conceição-Santos et al. (2020). This behavior means that the meridional and zonal tidal wind component is acting the most time over this station.

2. We observed three peaks in the *Es* layer behavior for all seasons, revealing that the terdiurnal tide (8-hour) can modulate their formation. This fact is very clear during the summer and spring. In summer, the 8-h modulation is controlled mainly by the *Es* layer occurrence in February, probably due to the terdiurnal tide having lower amplitudes in the summer onset. Although autumn shows an 8-h modulation in the *Es* layer occurrence, the first peak is not well-defined in March. During the winter, August has a poorly rate in the terdiurnal oscillation of the *Es* layer occurrence compared to June and July.

3. The 8-h modulation in the *Es* layer development over Palmas was confirmed using a nonlinear regression for each season. It is worth noting the 8-h periodicities in the fitted curves of the *Es* layer rates in all seasonal periods evidencing a possible effect of the terdiurnal tide on the development of *Es* layers. This behavior is less pronounced during the winter, agreeing with the maximum amplitudes of the terdiurnal tide occurring between 80 and 100 km of altitude in this season. Therefore, as the *Es* layer appeared above 100 km, we do not have an 8-h clearly on our data here.

4. The *ftEs* had lower values in the autumn and winter than those observed during the summer or spring months (below 10 MHz). Summer presented the highest *ftEs* values, that can be due to the Gradient Drift instability of the Equatorial Electrojet Current (EEJ), which is effective during the magnetic storms in the boundary equatorial magnetic sites, as is the case of the Palmas region. The disturbed electric fields can superimpose the wind shear mechanism during disturbed periods. As in this work, we do not separate the quiet and disturbed days, a more in-depth study of these *Es* layer development will be necessary,

and we intend to present it in the future. The month of February showed a prominent peak at ~20 UT of 14.9 MHz that may
315 be associated with the Sudden Stratospheric Warming (SSW) that occurred in early 2009 and had global influences on
atmospheric phenomena.

5. The results show that the densities of the *Es* layers simulated in MIRE are more intense when the terdiurnal tidal component
is added to the diurnal and semidiurnal tides, agreeing with the observations previously reported in work of Fytterer et al.
(2014).

Acknowledgments

PAF thanks Coordenação de Aperfeiçoamento de Pessoal de Nível Superior (CAPES) for student funding under grant number
88887.372542/2019-00. The authors thank the São Paulo Research Foundation (FAPESP) for the support received under grants
2019/19225-9, 2019/09361-2, 2016/22634-0, and for funding the São João do Cariri Meteor Radar which is operated in
cooperation of National Institute for Space Research (INPE) and the Campina Grande Federal University (UFCG). We also
325 thanks to Fundação de Pesquisa do Maranhão (FAPEMA), SECTI and the Government of the State of Maranhão, Brazil, for
partial funding of this research under process number BD-02689/20. MTAHM is grateful for the financial support received by
the Conselho Nacional de Desenvolvimento Científico e Tecnológico (CNPq) under process number 314261/2020-6. LCAR
and VFA thank the China-Brazil Joint Laboratory for Space Weather (CBJLSW), National Space Science Center (NSSC),
Chinese Academy of Sciences (CAS) for supporting their Postdoctoral fellowships. Finally, the authors thank Drs. Ricado
330 Buriti and Washington Lima for their efforts to continue the operation of the instruments at São João do Cariri and Palmas,
respectively.

References

Andrioli, V. F., Clemesha, B. R., Batista, P. P., and Schuch, N. J.: Atmospheric tides and mean winds in the meteor region
over Santa Maria (29.7°S; 53.8°W), *Journal of Atmospheric and Solar-Terrestrial Physics*, 71, 1864–1876,
https://doi.org/10.1016/j.jastp.2009.07.005, 2009.
335 Buriti, R. A., Hocking, W. K., Batista, P. P., Medeiros, A. F., and Clemesha, B. R.: Observations of equatorial mesospheric
winds over Cariri (7.4° S) by a meteor radar and comparison with existing models, *Annales Geophysicae*, 26, 485–497,
https://doi.org/10.5194/angeo-26-485-2008, 2008.
Carrasco, A. J., Batista, I. S., and Abdu, M. A.: Simulation of the sporadic E layer response to prereversal associated evening
vertical electric field enhancement near dip equator, *Journal of Geophysical Research: Space Physics*, 112, 1–10,
340 https://doi.org/10.1029/2006JA012143, 2007.

Conceição-Santos, F., Muella, M. T. A. H., Resende, L. C. A., Fagundes, P. R., Andrioli, V. F., Batista, P. P., and Carrasco, A. J.: On the role of tidal winds in the descending of the high type of sporadic layer (Es), *Advances in Space Research*, 65, 2131–2147, https://doi.org/10.1016/j.asr.2019.11.024, 2020.

345   Conceição-Santos, F., Muella, M. T. A. H., Resende, L. C. A., Fagundes, P. R., Andrioli, V. F., Batista, P. P., Pillat, V. G., and Carrasco, A. J.: Occurrence and Modeling Examination of Sporadic- E Layers in the Region of the South America (Atlantic) Magnetic Anomaly, *Journal of Geophysical Research: Space Physics*, 124, 9676–9694, https://doi.org/10.1029/2018JA026397, 2019.

Du, J., and Ward, W. E.: Terdiurnal tide in the extended Canadian Middle Atmospheric Model (CMAM), *Journal of Geophysical Research: Atmospheres*, 115, 1–21, https://doi.org/10.1029/2010JD014479, 2010.

350   Forbes, J. M., and Wu, D.: Solar Tides as Revealed by Measurements of Mesosphere Temperature by the MLS Experiment on UARS, *Journal of the Atmospheric Sciences*, 63, 1776–1797, https://doi.org/10.1175/JAS3724.1, 2006.

Forbes, J. M., Zhang, X., Palo, S., Russell, J., Mertens, C. J., and Mlynczak, M.: Tidal variability in the ionospheric dynamo region, *Journal of Geophysical Research: Space Physics*, 113, 1-17, https://doi.org/10.1029/2007JA012737, 2008.

Fuller-Rowell, T., Wang, H., Akmaev, R., Wu, F., Fang, T. W., Iredell, M., and Richmond, A.: Forecasting the dynamic and
355   electrodynamic response to the January 2009 sudden stratospheric warming, *Geophysical Research Letters*, 38, 1–6, https://doi.org/10.1029/2011GL047732, 2011.

Fytterer, T., Arras, C., Hoffmann, P., and Jacobi, C.: Global distribution of the migrating terdiurnal tide seen in sporadic E occurrence frequencies obtained from GPS radio occultations, *Earth, Planets and Space*, 66, 1-9, https://doi.org/10.1186/1880-5981-66-79, 2014.

360   Fytterer, T., Arras, C., and Jacobi, C.: Terdiurnal signatures in sporadic layers at midlatitudes, *Advances in Radio Science*, 11, 333–339, https://doi.org/10.5194/ars-11-333-2013, 2013.

Gao, S., and MacDougall, J. W.: A dynamic ionosonde design using pulse coding, *Canadian Journal of Physics*, 69, 1184–1189, https://doi.org/10.1139/p91-179, 1991.

Guharay, A., Batista, P. P., Clemesha, B. R., Sarkhel, S., and Buriti, R. A.: On the variability of the terdiurnal tide over a
365   Brazilian equatorial station using meteor radar observations, *Journal of Atmospheric and Solar-Terrestrial Physics*, 104, 87–95, https://doi.org/10.1016/j.jastp.2013.08.021, 2013.

Haldoupis, C.: Midlatitude Sporadic E. A Typical Paradigm of Atmosphere-Ionosphere Coupling, *Space Science Reviews*, 168, 441–461, https://doi.org/10.1007/s11214-011-9786-8, 2012.

Haldoupis, C., and Pancheva, D.: Terdiurnal tidelike variability in sporadic E layers, *Journal of Geophysical Research*, 111,
370   1–10, https://doi.org/10.1029/2005JA011522, 2006.

Haldoupis, C., Pancheva, D., and Mitchell, N. J.: A study of tidal and planetary wave periodicities present in midlatitude sporadic E layers, *Journal of Geophysical Research: Space Physics*, 109, 1–12, https://doi.org/10.1029/2003JA010253, 2004.

Hocking, W. K.: Radar meteor decay rate variability and atmospheric consequences, *Annales Geophysicae*, 22, 3805–3814, https://doi.org/10.5194/angeo-22-3805-2004, 2004.

375   Huang, J., and MacDougall, J. W.: Legendre coding for digital ionosondes, *Radio Science*, 40, 1–11, https://doi.org/10.1029/2004RS003123, 2005.

Jacobi, C., and Arras, C.: Tidal wind shear observed by meteor radar and comparison with sporadic E occurrence rates based on GPS radio occultation observations, *Advances in Radio Science*, 17, 213–224, https://doi.org/10.5194/ars-17-213-2019, 2019.

380   Jin, H., Miyoshi, Y., Pancheva, D., Mukhtarov, P., Fujiwara, H., and Shinagawa, H.: Response of migrating tides to the stratospheric sudden warming in 2009 and their effects on the ionosphere studied by a whole atmosphere-ionosphere model GAIA with COSMIC and TIMED/SABER observations, *Journal of Geophysical Research: Space Physics*, 117, 1–20, https://doi.org/10.1029/2012JA017650, 2012.

Kirkwood, S., and Nilsson, H.: High-latitude sporadic-e and other thin layers – the role of magnetospheric electric fields, 385   *Space Science Reviews*, 91, 579–613, https://doi.org/10.1023/A:1005241931650, 2000.

Lieberman, R. S., Oberheide, J., and Talaat, E. R.: Nonmigrating diurnal tides observed in global thermospheric winds, *Journal of Geophysical Research: Space Physics*, 118, 7384–7397, https://doi.org/10.1002/2013JA018975, 2013.

Lilienthal, F., Jacobi, C., and Geißler, C.: Forcing mechanisms of the terdiurnal tide, *Atmospheric Chemistry and Physics*, 18, 15725–15742, https://doi.org/10.5194/acp-18-15725-2018, 2018.

390   Lin, J. T., Lin, C. H., Chang, L. C., Huang, H. H., Liu, J. Y., Chen, A. B., Chen, C. H., and Liu, C. H.: Observational evidence of ionospheric migrating tide modification during the 2009 stratospheric sudden warming, *Geophysical Research Letters*, 39, 2–7, https://doi.org/10.1029/2011GL050248, 2012.

Liu, H. L., and Roble, R. G.: A study of a self-generated stratospheric sudden warming and its mesospheric-lower thermospheric impacts using the coupled TIME-GCM/CCM3, *Journal of Geophysical Research Atmospheres*, 107, 1-18, 395   https://doi.org/10.1029/2001JD001533, 2002.

McLandress, C.: The Seasonal Variation of the Propagating Diurnal Tide in the Mesosphere and Lower Thermosphere. Part I: The Role of Gravity Waves and Planetary Waves, *Journal of the Atmospheric Sciences*, 59, 893–906, https://doi.org/10.1175/1520-0469(2002)059<0893:TSVOTP>2.0.CO;2, 2002a.

McLandress, C.: The Seasonal Variation of the Propagating Diurnal Tide in the Mesosphere and Lower Thermosphere. Part 400   II: The Role of Tidal Heating and Zonal Mean Winds, *Journal of the Atmospheric Sciences*, 59, 907–922, https://doi.org/10.1175/1520-0469(2002)059<0907:TSVOTP>2.0.CO;2, 2002b.

Moudden, Y., and Forbes, J. M.: A decade-long climatology of terdiurnal tides using TIMED/SABER observations, *Journal of Geophysical Research: Space Physics*, 118, 4534–4550, https://doi.org/10.1002/jgra.50273, 2013.

Oikonomou, C., Haralambous, H., Haldoupis, C., and Meek, C.: Sporadic E tidal variabilities and characteristics observed 405   with the Cyprus Digisonde, *Journal of Atmospheric and Solar-Terrestrial Physics*, 119, 173–183, https://doi.org/10.1016/j.jastp.2014.07.014, 2014.

Pancheva, D., Mukhtarov, P., and Smith, A. K.: Climatology of the migrating terdiurnal tide (TW3) in SABER/TIMED temperatures, *Journal of Geophysical Research: Space Physics*, 118, 1755–1767, https://doi.org/10.1002/jgra.50207, 2013.

Pillat, V. G., Guimarães, L. N. F., Fagundes, P. R., and Silva, J. D. S.: A computational tool for ionosonde CADI's ionogram

410   analysis. *Computers & Geosciences*, 52, 372–378, https://doi.org/10.1016/j.cageo.2012.11.009, 2013.

Plane, J. M. C.: Atmospheric Chemistry of Meteoric Metals, *Chemical Reviews*, 103, 4963–4984, https://doi.org/10.1021/cr0205309, 2003.

Resende, L. C. A., Batista, I. S., Denardini, C. M., Batista, P. P., Carrasco, A. J., Andrioli, V. de F., and Moro, J.: Simulations of blanketing sporadic E-layer over the Brazilian sector driven by tidal winds, *Journal of Atmospheric and Solar-Terrestrial*

415   *Physics*, 154, 104–114, https://doi.org/10.1016/j.jastp.2016.12.012, 2017a.

Resende, L. C. A., Batista, I. S., Denardini, C. M., Batista, P. P., Carrasco, A. J., Andrioli, V. F., and Moro, J.: The influence of tidal winds in the formation of blanketing sporadic E-layer over equatorial Brazilian region, *Journal of Atmospheric and Solar-Terrestrial Physics*, 171, 64–71, https://doi.org/10.1016/j.jastp.2017.06.009, 2017b.

Resende, L. C. A., Batista, I. S., Denardini, C. M., Carrasco, A. J., de Fátima Andrioli, V., Moro, J., Batista, P. P., and Chen,

420   S. S.: Competition between winds and electric fields in the formation of blanketing sporadic E layers at equatorial regions, *Earth, Planets and Space*, 68, 1–14, https://doi.org/10.1186/s40623-016-0577-z, 2016.

Smith, A. K.: Global Dynamics of the MLT, *Surveys in Geophysics*, 33, 1177–1230, https://doi.org/10.1007/s10712-012-9196-9, 2012.

Venkateswara Rao, N., Tsuda, T., Gurubaran, S., Miyoshi, Y., and Fujiwara, H.: On the occurrence and variability of the

425   terdiurnal tide in the equatorial mesosphere and lower thermosphere and a comparison with the Kyushu-GCM, *Journal of Geophysical Research*, 116, 1–13, https://doi.org/10.1029/2010JD014529, 2011.

Piggott, W. R., Rawer, K.: U.R.S.I. handbook of ionogram interpretation and reduction, In *World Data Center A for Solar-Terrestrial Physics*, WDC-A report UAG-23: NOAA, https://repository.library.noaa.gov/view/noaa/1013, 1972.

Wang, H., Fuller-Rowell, T. J., Akmaev, R. A., Hu, M., Kleist, D. T., and Iredell, M. D.: First simulations with a whole

430   atmosphere data assimilation and forecast system: The January 2009 major sudden stratospheric warming, *Journal of Geophysical Research: Space Physics*, 116, 1–6, https://doi.org/10.1029/2011JA017081, 2011.

Whitehead, J. D.: The formation of the sporadic-E layer in the temperate zones, *Journal of Atmospheric and Terrestrial Physics*, 20, 49–58, https://doi.org/10.1016/0021-9169(61)90097-6, 1961.

Whitehead, J. D.: Recent work on mid-latitude and equatorial sporadic-E, *Journal of Atmospheric and Terrestrial Physics*,

435   51, 401–424, https://doi.org/10.1016/0021-9169(89)90122-0, 1989.

Zhao, G., Liu, L., Ning, B., Wan, W., and Xiong, J.: The terdiurnal tide in the mesosphere and lower thermosphere over Wuhan (30°N, 114°E), *Earth, Planets and Space*, 57, 393–398, https://doi.org/10.1186/BF03351823, 2005.